Science Robotics
AAAS

robotics.sciencemag.org/cgi/content/full/6/50/eabb9138/DC1

Supplementary Materials for

A system of coordinated autonomous robots for Lagrangian studies of microbes in the oceanic deep chlorophyll maximum

Yanwu Zhang*, John P. Ryan, Brett W. Hobson, Brian Kieft, Anna Romano, Benedetto Barone, Christina M. Preston, Brent Roman, Ben-Yair Raanan, Douglas Pargett, Mathilde Dugenne, Angelicque E. White, Fernanda Henderikx Freitas, Steve Poulos, Samuel T. Wilson, Edward F. DeLong, David M. Karl, James M. Birch, James G. Bellingham, Christopher A. Scholin

*Corresponding author. Email: yzhang@mbari.org

Published 13 January 2021, *Sci. Robot.* **6**, eabb9138 (2021)
DOI: 10.1126/scirobotics.abb9138

This PDF file includes:

Method for computing average profiles of physical, chemical, and bio-optical conditions at Station ALOHA

To represent the typical structure of the DCM and the underlying distributions of density, photosynthetic pigments, nutrients, and light in the water column of the study region (Figure 1A), we computed climatological average profiles from the Hawaii Ocean Time-series (HOT) observations at Station ALOHA (22°45'N, 158°W; Figure 1B). All analyses were constrained to March-April, the months of our study. The average profiles of potential density anomaly, chloropigment (chlorophylls+phaeopigments), and nitrate+nitrite concentrations were computed from measurements from March 1990 to April 2018; the average photosynthetically active radiation (PAR) profile was computed from measurements from March 1998 to April 2009.

Method for computing statistical summaries from profiles of chloropigment and particulate beam attenuation coefficient from shipboard CTD rosette measurements

To evaluate whether the DCM coincided with a local maximum in particle concentrations in the water column within the cyclonic eddy, we examined profiles of calibrated measurements of chloropigment (chlorophylls+phaeopigments [66]) and optical beam attenuation [75] [76] measured respectively by the fluorometer and the transmissometer installed on the shipboard CTD rosette. Beam attenuation coefficient was averaged within the depth range 380 to 400 m, then subtracted from the profile to represent particulate beam attenuation coefficient (c_p) within the overlying water column. For each leg (16 profiles from leg 1; 37 profiles from leg 2), the mean and standard deviation (sd) of c_p were computed within isopycnal layers using data from the upper 200 m, represented as the mean profile with a 1 sd envelope (Figure S1).

Methods for ship-based current velocity measurement and comparison with drift velocities

An OS75 Acoustic Doppler Current Profiler (ADCP) (Teledyne RD Instruments, Poway, CA) was installed on R/V *Falkor*. The ADCP operated at 75 kHz and measured current velocity between ~24 and 500 m depths in 8-m bins. The ADCP data were logged at 5-minute intervals. Earth-referenced current velocity was derived from the water velocity relative to the ADCP, and the ship (ADCP) velocity relative to the Earth (from GPS position). Velocity data from the ADCP were used for two purposes. The first was to compare the velocity of the drifting *Aku* with ADCP-measured current velocity at the depth of *Aku*. Because the eddy created substantial velocity gradients (Figure 3A), this comparison was constrained to ADCP velocity measurements within 5 km of *Aku*. Sufficient data for comparison were acquired during three periods of each sampling leg (Figure S2). The Wilcoxon rank-sum test showed that speed estimates from matched segments of ship ADCP measurements and *Aku* drift trajectory (Figure S2) were equivalent (median speeds of 0.24 and 0.25 m/s, respectively; $p = 0.48$). Bartlett's test of homogeneity of variances did not reject the null hypothesis of equal variances (standard deviations of 0.05 m/s for both platforms; $p = 0.97$), therefore Student's t-test was the appropriate parametric test for equivalence of means. The t-test did not reject the null hypothesis of equivalence of means (0.22 and 0.25 m/s, respectively; $p = 0.42$). The second purpose was to examine the current speed profile from near-surface to the 120-m drogue depth of the drifter (Figure S3), using ADCP velocity measurements acquired within 5 km of the drifter.

Methods for shipboard sampling for RNA analysis

The CTD rosette carried a fluorometer and transmitted the real-time chlorophyll fluorescence and temperature profiles to the shipboard lab via the electro-mechanical cable. DCM sampling followed the same principle as that used by the sampling LRAUV. At the first CTD rosette sampling station of each leg, the scientists visually inspected the profiles and determined the isotherm that corresponded to the

DCM chlorophyll peak. At successive sampling stations of each leg, a Niskin bottle was manually triggered at the depth of the targeted isotherm to acquire the DCM water sample.

Shipboard samples for RNA analysis were collected at 50-m depth, DCM, and 250-m depth using the CTD rosette deployed at 06:00, 12:00, and 18:00 HST (Hawaii Standard Time) for 18 time points per leg. Seawater collected in Niskin bottles was filtered to collect and estimate particulate RNA transcripts. Two liters of seawater per depth were filtered through stacked 5 μm and 0.22 μm filters (the same pore sizes as those of the ESP filters) housed in a Swinnex filter holder (MilliporeSigma, Burlington, MA), that was attached to Masterflex tubing L/S 15 (Cole Parmer, Vernon Hills, IL) fed through a peristaltic single channel head. The peristaltic pump speed was set to 80 mL/minute. Duplicate filters were collected per time point and depth. Filters were removed from the Swinnex holder using ethanol cleaned forceps and placed in polymerase chain reaction (PCR) clean 2.0 mL tubes with 0.3 mL RNAlater. Filters were coated with RNAlater and left for approximately 10 minutes prior to storing at -80˚C. Filtration volumes were measured with a 2 L graduated cylinder.

Methods for RNA extraction from shipboard and ESP samples

The 0.22 μm filters from ship and ESP sampling were stored on ice upon removal from -80°C storage. The samples were centrifuged at 2000 rcf for 30 seconds prior to removal of RNAlater. A total of 300 μL of denaturing solution lysis buffer (Ambion, Inc., Austin, TX) was added to each filter, vortexed for 1 minute, and then stored on ice. Next, to target 1% of total sample reads, 2 μL of diluted (1/100) ERCC "spike in" RNA standards (ThermoFisher Scientific, Hampton, NH) were added to the lysate prior to purification with 898 μL of nuclease free water (Ambion, Inc.). RNA purification was performed using the Magnetic Separation Module (MSM) instrument with a 96-rod head (PerkinElmer, Waltham, MA). Into each sample well, 650 μL of sample were loaded in duplicate, and the instrument was loaded with MSM reagents from Tissue RNA kit (CMG-1212, PerkinElmer), and 80 μL DNA free magnetic beads were added to each sample well. Samples were DNase treated on board the instrument during the purification protocol. After magnetic bead purification, samples were eluted with 50 μL of RNase free water. RNA eluates were spilt into two plates and sealed for long-term storage at -80°C. A 6-μL aliquot (stored at -80°C) was reserved for RNA quality and quantification tests.

Methods for shipboard sampling for conventional and imaging flow cytometry and statistical analysis

Estimates of phytoplankton cell concentration across the water column were made by coupling conventional (Influx Cell Sorter flow cytometer, BD Biosciences, San Jose, CA) and imaging flow cytometry (IFCB, McLane Research and Laboratories, Inc., East Falmouth, MA). The two instruments offer complementary data sets comprising cell counts and optical fingerprints of photosynthetic picoeukaryotes (PPEs) in the size range 0.8-3 μm and larger phytoplankton (4-100 μm) respectively.

For conventional flow cytometry, shipboard samples were collected at HOT standard depths (5, 25, 45, 75, 100, 125, 150, 175 m) using the CTD rosette deployed at 02:00, 04:00, 16:00, and 22:00 HST for legs 1 and 2. One-mL samples were fixed with paraformaldehyde (0.2 μm syringe filtered; 0.25% final concentration) in the dark at room temperature for 15 minutes prior to flash freezing in liquid nitrogen and stored at -80°C. Both light scattering and autofluorescence emission of cells' photopigments were recorded as individual cells passed through a 200 mW 488 nm laser. PPEs were identified based on their optical fingerprints (light scatter and fluorescence emission) and subsequently counted using the acquisition software Spigot (BD Biosciences).

For imaging flow cytometry, shipboard samples were collected at the DCM and within the mixed layer (5 and 15 m) during leg 2 only from the CTD rosette deployed at 06:00, 12:00, and 18:00 HST. Samples of 5

mL were analyzed within 3 hours after collection to acquire high resolution images used to identify phytoplankton cells and subsequently count the total cell concentration of phytoplankton larger than 4 µm. For each sample, cells (including photosynthetic and non-photosynthetic species) were manually classified at the genera level and annotated as either autotrophs or heterotrophs based on the literature.

PPE and corresponding chloropigment concentrations were examined for two purposes. The first was to evaluate whether the DCM represented a local maximum in PPE concentrations within the water column. The second was to test whether chloropigment and PPE concentrations within the DCM decreased between the first and second sampling legs. Neither variable was normally distributed (Shapiro-Wilk normality test, $p < 0.05$), thus the non-parametric two-sample Wilcoxon rank-sum test was applied to test significance of the differences.

Methods for sea-surface PAR measurement and statistical analysis

Photosynthetically active radiation (PAR) levels at the sea surface during the two DCM sampling legs were measured by a LI-1500 Light Sensor Logger (LICOR, Lincoln, NE) installed on the deck of R/V *Falkor*. The PAR data were logged at 1-minute intervals. We calculated the daily average PAR levels (from midnight to midnight) of 16-20 March for leg 1 and those of 28 March to 1 April for leg 2. The null hypothesis that the means of the daily average PAR levels during DCM sampling on legs 1 and 2 were equal was not rejected (Student's t-test, $p = 0.91$; following Levene's test, $p = 0.45$, hence the null hypothesis of equal variances was not rejected). We used software R (release 3.5.3; http://www.R-project.org/) for statistical analysis.

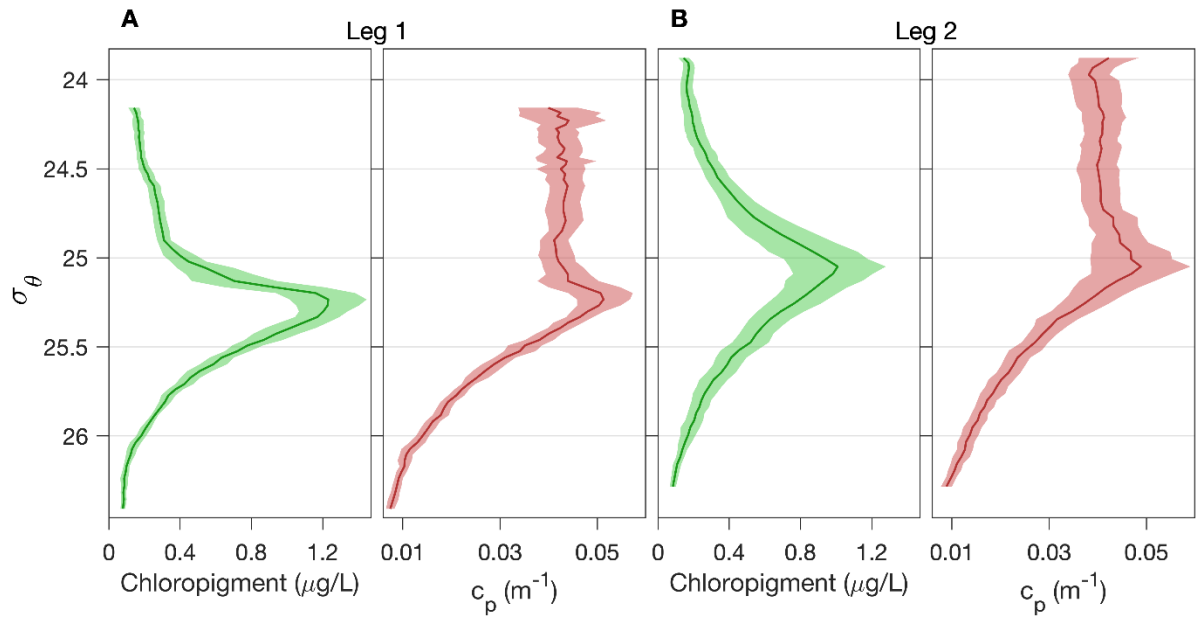

Fig. S1. Ship-based characterization of the deep chlorophyll maximum. Profiles of the mean and envelope (± one standard deviation) of chloropigment (chlorophylls + phaeopigments) and particulate beam attenuation coefficient (c_p) during sampling legs 1 (A) and 2 (B).

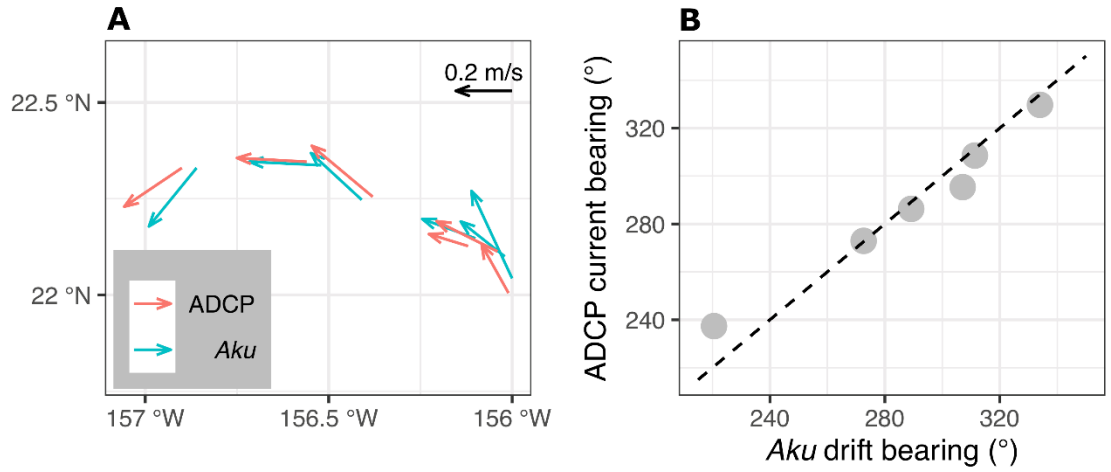

Fig. S2. Lagrangian drift velocities. (A) *Aku* drift velocity compared with nearby (3.9 ± 0.8 km in leg 1 and 3.7 ± 0.9 km in leg 2) Earth-referenced horizontal current velocity measured by R/V *Falkor* shipboard Acoustic Doppler Current Profiler at the depth of *Aku* in sampling leg 1 (east of 156.25ºW) and leg 2 (west of 156.25ºW). (B) Scatter plot of the bearings of each pair of velocity vectors in (A). The 1:1 dashed line is shown for reference.

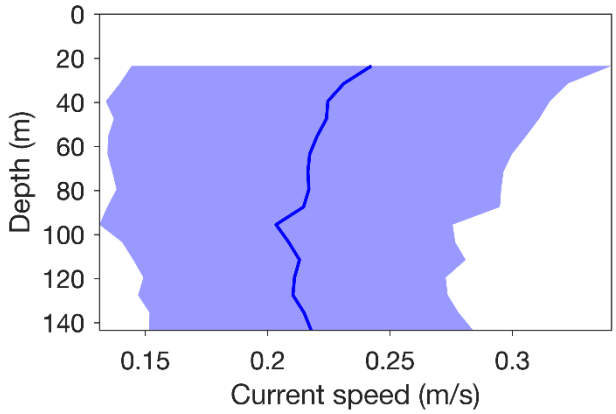

Fig. S3. Vertical variation of horizontal current speed. Profile of the mean and envelope (± one standard deviation) of Earth-referenced horizontal current speed (measured by R/V *Falkor* shipboard Acoustic Doppler Current Profiler) averaged over locations near the drogued drifter (3.1 ± 1.1 km in leg 1 and 3.2 ± 1.1 km in leg 2).

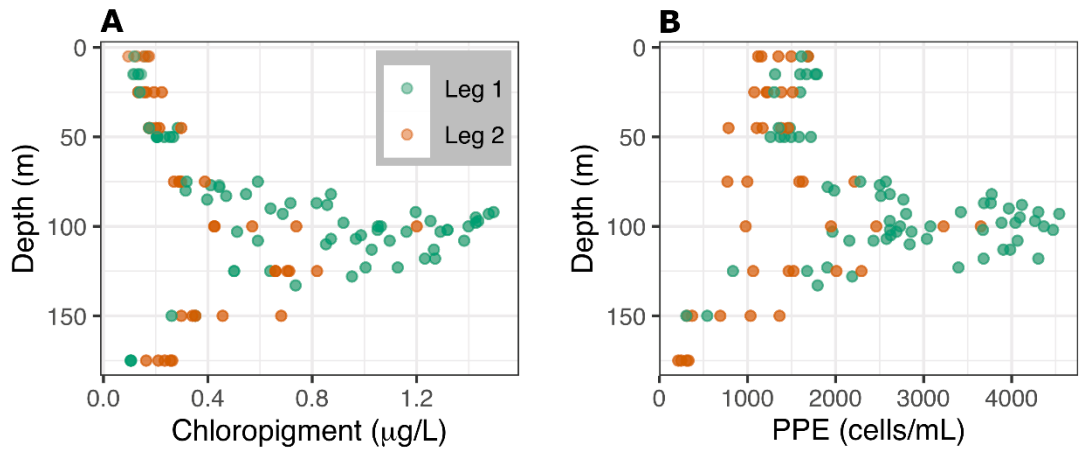

Fig. S4. Water-column biomass characterization. Concentrations of (A) chloropigment (chlorophylls + phaeopigments) and (B) photosynthetic picoeukaryotes (PPEs) from ship conductivity-temperature-depth rosette samples in legs 1 and 2.

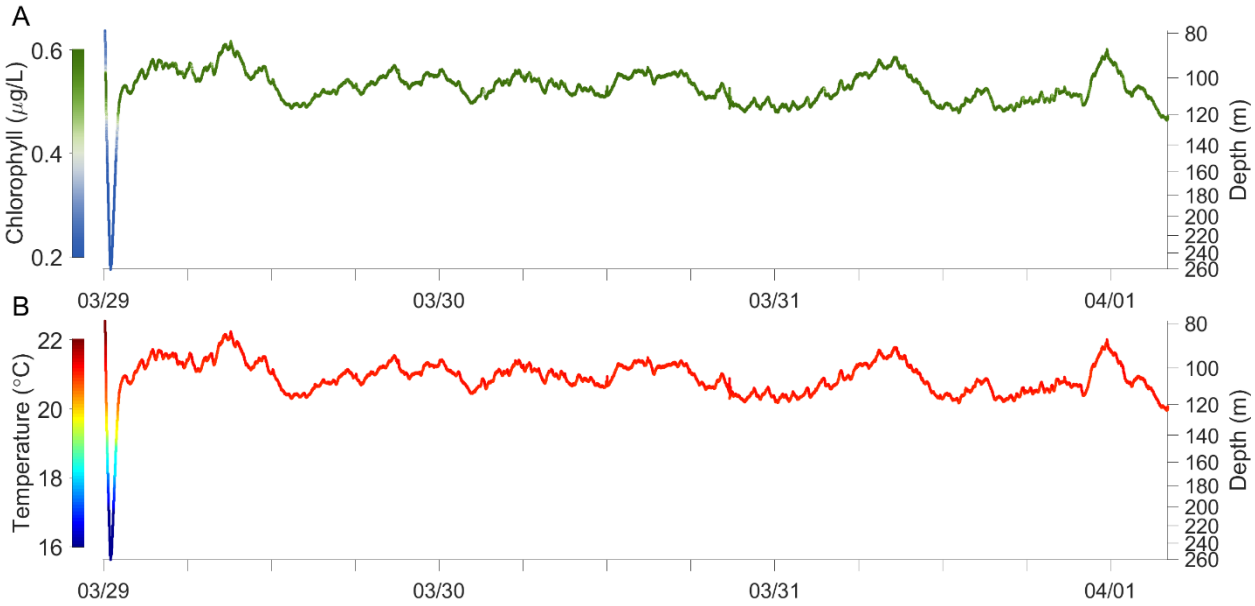

Fig. S5. Localization of the deep chlorophyll maximum (DCM) followed by Lagrangian drift within the DCM. Fluorescence-derived chlorophyll (A) and temperature (B) measured by *Aku* during leg 2. *Aku* descended from the surface to 260-m depth to find the peak of the chlorophyll signal in the water column and the corresponding temperature. It then ascended to reach the recorded chlorophyll-peak associated temperature, and thereafter actively adjusted its depth to remain at that temperature so as to track the DCM (Figure 4). Time is UTC.